




Photophysical Studies on D- π -A Imidazole Derivative for Organic Dye Sensitized Solar Cell Application

SHASHIKANT WALKI¹, HEMANTKUMAR M. SAVANUR², M.K. RAVINDRA¹,
SONIYA NAIK³, G.H. MALIMATH⁴, K.M. MAHADEVAN¹ and LOHIT NAIK^{4,*} 

¹Department of Chemistry, Kuvempu University, P.G. Centre Kadar, Shivamoga-577548, India

²Department of Chemistry, Karnataka Science College, Dharwad-580001, India

³Department of Chemistry, IIT Bombay, Powai, Mumbai-400076, India

⁴Department of Physics, Karnataka Science College, Dharwad-580001, India

*Corresponding author: E-mail: lohitresearch@gmail.com

Received: 9 June 2020;

Accepted: 20 July 2020;

Published online: 28 October 2020;

AJC-20105

In present study, a new organic dye 2-(4-chlorophenyl)-1-(4-methoxyphenyl)-4,5-diphenyl-1H-imidazole (CMI) containing phenyl donor with imidazole ring as π -linker and chlorophenyl group as acceptor have been synthesized. The photophysical properties like solvatochromism, optical band gap and fluorescence lifetime are estimated using experimental as well as quantum chemical computational techniques. Further, photosensitization of TiO₂ nanoparticles from CMI dye has been investigated using absorption, steady-state and time resolved fluorescence methods. The increase in absorbance and a decrease in fluorescence spectra with different concentrations of TiO₂ nanoparticles confirmed the possibility of interactions between dye and TiO₂ nanoparticles. Rehm-Weller relation suggests that a decrease in fluorescence of CMI dye was due to photo-induced electron transfer process and the Stern-Volmer studies suggest that the fluorescence quenching mechanism was due to combined dynamic and static quenching process. Further, dye-sensitized solar cell using this newly synthesized CMI dye has been fabricated and characterized for their photovoltaic performance under illumination. Photovoltaic energy conversion efficiency and fill factor of the CMI dye were found to be 1.76% and 0.56, respectively.

Keywords: Imidazoles derivatives, TiO₂ nanoparticles, Fluorescence quenching, Dye sensitized solar cell.

INTRODUCTION

Solar energy is the source of nearly all energies on earth. Among all the renewable power sources, solar energy is the most inexhaustible, quiet, easily exploitable and adjustable to enormous applications. In recent years, the major research work is carried out on the synthesis of novel dyes that serve as light absorbers in solar cells. The molecular composition of the organic dyes plays an important role in the performance of dye sensitized solar cells (DSSCs). The structural components of organic sensitizers suitable for DSSCs can be divided into three categories: donor (D), π -linker and acceptor with an anchoring (A) group [1,2].

A large number of organic dyes containing nitrogenous electron donors such as carbazole, phenothiazine, coumarin, triphenylamine, amine-substituted indoline, fluoreneamine and thienoindole have been used with great success in DSSCs [3-14]. The π -conjugated linker in a D- π -linker-A system besides

being a part of the light absorbing chromophore functions as a molecular wire for electron transfer from the donor to acceptor. Various aromatic/ heteroaromatic units such as naphthalene, dihydrophenanthrene, fluorene, spirobifluorene, anthracene, oligothiophene, thienothiophene, dithienothiophene, carbazole, phenoxazine, phenothiazine, benzothiadiazole and benzotriazole have been explored as π -linkers between the electron donor and electron acceptor for tuning the absorption, electrochemical and other characteristics required for DSSC performance [15-39]. Triarylamine containing imidazoles [40-42] or fused aromatic imidazoles such as phenanthromidazole [43,44] and pyrenoimidazole [45,46] have also been found to serve as promising donors when connected with oligothiophene units.

In view of the above, the synthesis and characterization of the novel donor-acceptor substituted imidazole derivative using experimental and theoretical methods is reported and discussed.

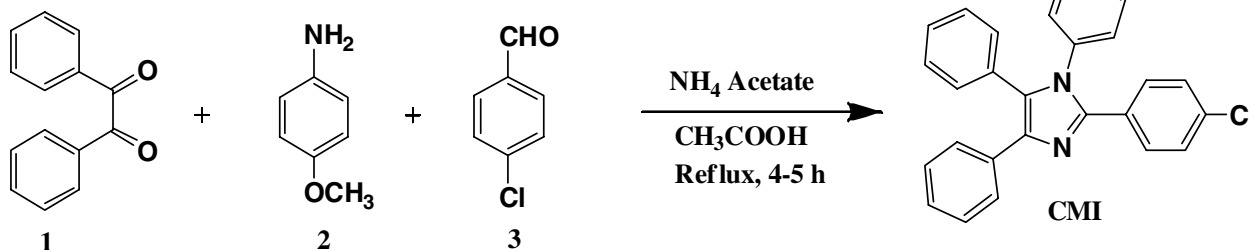
EXPERIMENTAL

Chemicals and reagents used for the synthesis and analysis were procured from Sigma-Aldrich, India. Analytical grade solvents were purchased from Lobachemie. Pvt Ltd., India. The melting point was measured on a Boetius-Mikroheiztisch. TLC was performed by using aluminium foil fluorescent indicator from Merck KGaA (silica gel 60 F₂₅₄, layer thickness 0.2 mm). ¹H & ¹³C NMR spectrum were recorded using a JEOL with 100 MHz operating frequency deuterated chloroform (CDCl₃) solvents. IR spectra were of the dyes recorded using Nicolet 5700 FT-IR instrument.

Fluorescence lifetime measurements were carried out using an ISS ChronoBH time correlated single photon counting spectrometer. A pulsed light emitting diode with excitation wavelength 340 nm was used as an excitation source. Cyclic voltammetry (CV) studies were carried out using an electrochemical analyzer/Work station (model: CHI112C, series, USA) at 0.1 M tetrabutylammonium hexafluorophosphate (TBAPF₆) as supporting electrolyte with a scan rate 1 × 10⁻³ V s⁻¹.

Computational details: The optimized molecular geometry of the synthesized dyes was estimated by DFT calculations using B3LYP/6-31G basis set as implemented in the Gaussian 09 program package [47].

Synthesis of 2-(4-chlorophenyl)-1-(4-methoxyphenyl)-4,5-diphenyl-1H-imidazole (CMI): In a 250 mL round-bottom flask, a 4-methoxy aniline (1 mmol, 0.123 g), benzil (1 mmol, 0.210 g), ammonium acetate (1 mmol, 0.75 g) and 4-chloro benzaldehyde (1 mmol, 0.140 g) were taken in glacial acetic acid (20 mL). The reaction mixture was then subjected to ultrasonication for 30 min and kept it for reflux for 4-5 h on heating mantle. The progress of the reaction was monitored by TLC (2:8 ethyl acetate:petroleum ether). After the completion of the reaction, the mixture was cooled to room temperature and poured into ice-cold water. The reaction mixture was neutralized by aqueous sodium bicarbonate solution and the product was extracted with ethyl acetate. The crude product recrystallized by hot chloroform and ethyl acetate (2:6) to get a pure 2-(4-chlorophenyl)-1-(4-methoxyphenyl)-4,5-diphenyl-1H-imidazole (CMI) with good yield (70-80%) (**Scheme-I**). Light yellow colour solid, m.p.: 186-188 °C; IR (KBr, ν_{max}, cm⁻¹): 656 (C-Cl), 1251 (C-N), 1527 (Ar, C=C), 1593 (C=N), 2857 (aliph. C-H), 2927 (Ar-H). ¹H NMR (400 MHz, CDCl₃, δ ppm): 7.59-7.53 (m, 2H), 7.42-7.35 (m, 2H), 7.29-7.19 (m, 8H), 7.14-7.08 (m, 2H), 6.98-6.92 (m, 2H), 6.79-6.72 (M, 2H), 3.77 (s,



Scheme-I: Synthetic route for construction of 2-(4-chlorophenyl)-1-(4-methoxyphenyl)-4,5-diphenyl-1H-imidazole (CMI)

3H). ¹³C NMR (100 MHz, CDCl₃, δ ppm): 55.47, 114.4, 126.6, 127.45, 127.43, 128.11, 128.28, 128.480, 129.44, 130.15, 131.18.

RESULTS AND DISCUSSION

The normalized absorption spectra of CMI dye in different solvents is shown in Fig. 1 and the value of wavelength at absorption maxima is given in Table-1. It is observed that the excitation maxima of dye in a variety of solvents lies between 307 and 331 nm. On changing the media from non-polar to polar solvents CMI molecule shows a redshift of 24 nm. The results revealed that the solvents environment strongly enhances the intra molecular charge transfer and there was a possibility of $\pi \rightarrow \pi^*$ transition.

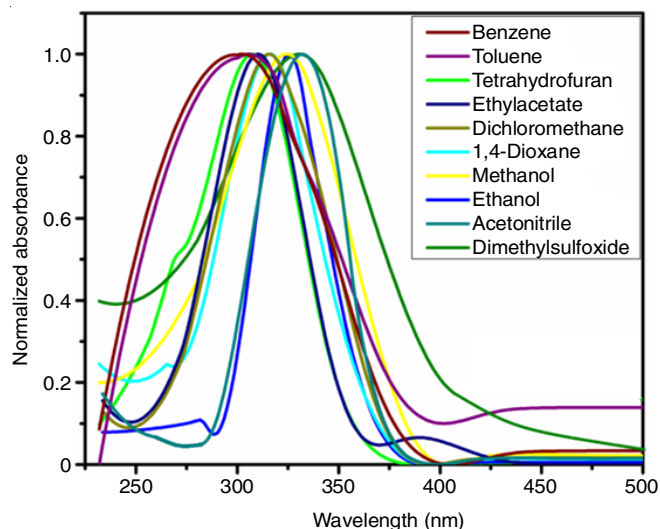


Fig. 1. Normalised absorption spectra of CMI dye in different solvents

The normalized fluorescence spectra of CMI dye in different solvents is shown in Fig. 2. The fluorescence spectra of CMI dye was recorded using wavelength ($\lambda_{\text{max}}^{\text{abs}}$) at absorption maxima in different solvents and the value of wavelength at fluorescence maxima ($\lambda_{\text{max}}^{\text{emi}}$) is given in Table-1. It is observed that the fluorescence maxima of CMI dye show 444 nm for benzene and 475 nm for DMSO. The large solvatochromic shift between these two solvents was due to the dielectric constant. The values of Stoke shift varies with respect to the solvent environment giving an account of the specific interaction between the solute and solvent molecules. The less pronounced shift in the

TABLE-1
PHOTOPHYSICAL PARAMETERS OF CMI DYE

Solvent	$\lambda_{\text{max}}^{\text{abs}}$ (nm)	$\lambda_{\text{max}}^{\text{emi}}$ (nm)	$\Delta\lambda$ (nm)	Quantum yield	Fluorescence lifetime $\langle t \rangle$ (ns)	k_r ($\times 10^9$)	k_{nr} ($\times 10^9$)
Benzene	307	444	137	0.561	2.830	0.198	1.584
Toulene	308	448	140	0.585	2.860	0.205	1.505
Tetrahydro furan	308	449	141	0.586	2.860	0.205	1.502
Ethyl acetate	309	452	143	0.589	2.880	0.205	1.493
Dichloromethane	315	457	142	0.603	2.910	0.207	1.451
1,4-Dioxane	316	459	143	0.609	2.940	0.207	1.435
Methanol	323	460	137	0.632	2.950	0.214	1.368
Ethanol	325	462	137	0.635	2.970	0.214	1.361
Acetonitrile	329	463	134	0.631	2.980	0.212	1.373
Dimethyl sulfoxide	331	475	145	0.639	2.980	0.214	1.351

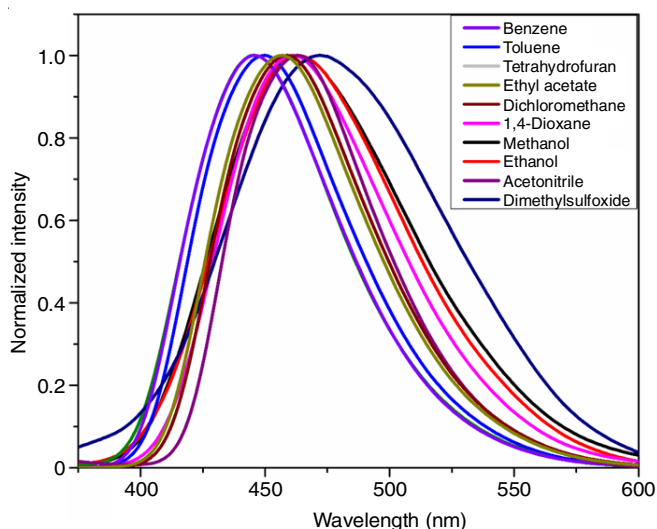


Fig. 2. Normalized fluorescence spectra of CMI dye in different solvents

absorption spectra of CMI dye in all the solvents is due to the less polar nature of the CMI dye in the ground state than in the excited state.

In order to design an optoelectronic device like, dye sensitized solar cell (DSSC), organic light emitting diodes (OLED's), etc. one has to knowledge about the optical band gap and it gives the information about electronic excitation energy levels of the organic material. In electronic transitions, the dye absorbs photon in UV-visible spectral range and promote an electron from the highest occupied molecular orbital (HOMO) to lowest unoccupied molecular orbital (LUMO) [48] and this can observe

with the help of UV-Vis spectrophotometer. The optical band gap (E_g) is determined from the onset of the low energy side of the experimentally recorded absorption spectra (λ_{onset}) using eqn. 1 and the values of the optical band gap [48] in different solvents is given in Table-2.

$$E_g = \frac{1240}{\lambda_{\text{onset}}} \quad (1)$$

Table-2 showed that on changing solvent media from non-polar to polar, optical band decreased from 3.543 eV to 3.255 eV. This may be due to the formation of a hydrogen bond between methoxy functional group of dye to the solvent environment and this effect increase with increase in dielectric constant and the excited state is more polar as compared with the ground state.

The fluorescence quantum yield (ϕ_s) [49] of the CMI dye was experimentally determined by comparing with the standard fluorescent dye of known quantum yield [POPOP laser dye ($\phi_R = 0.97$)] using following eqn. 2 in different solvents and the values are given in Table-1.

$$\phi_s = \phi_R \frac{I_s OD_R n_s^2}{I_R OD_s n_R^2} \quad (2)$$

where, ϕ , I, OD and n represent quantum yield, integrated fluorescence intensity, optical density and refractive index, while S and R represent the sample and reference, respectively. From Table-1, it was observed that the synthesized CMI dye having good quantum yield and highly fluorescent. This is a necessary and most important property of a dye in order to explore

TABLE-2
VALUES OF HOMO-LUMO AND CHEMICAL HARDNESS

Solvent	Experimental calculation	Theoretical calculation			
	Optical band gap E_g (eV)	HOMO (eV)	LUMO (eV)	Energy band gap E_g (eV)	η
Benzene	3.543	-5.867	-2.643	-3.224	1.612
Toluene	3.503	-5.815	-2.629	-3.186	1.593
Tetrahydrofuran	3.464	-5.784	-2.601	-3.183	1.542
Ethyl acetate	3.444	-5.685	-2.572	-3.113	1.522
Dichloromethane	3.397	-5.715	-2.571	-3.144	1.632
1,4-Dioxane	3.388	-5.734	-2.611	-3.123	1.562
Methanol	3.324	-5.634	-2.451	-3.183	1.592
Ethanol	3.307	-5.534	-2.364	-3.17	1.585
Acetonitrile	3.272	-5.615	-2.456	-3.159	1.650
Dimethyl sulfoxide	3.255	-5.688	-2.504	-3.184	1.537

in the field of optoelectronics. The values of quantum yield of CMI dye in different solvent is given in Table-1. It is observed that quantum yield of CMI dye varies from 0.561 to 0.639. The change in quantum yield may be due to the formation of a hydrogen bond between methoxy functional group of dye to the solvent environment.

Further from the knowledge of quantum yield and average life time, radiative rate (k_r) and non-radiative rate constant (k_{nr}) were calculated using eqns. 3 and 4:

$$k_r = \frac{\phi_s}{\tau_0} \quad (3)$$

and the non-radiative decay rate constant is given by:

$$k_{nr} = \frac{1}{\tau_0} - k_r \quad (4)$$

The values of radiative and non-radiative rate constant of CMI dye in different solvents are given in Table-1. Using pulsed excitation energy source, the dye molecule can be excited to its excited state in solvent media. In the excited state, dye molecule interacted with the surrounding solvent molecule before returning to the ground state. These excited state solute-solvent interactions influence the fluorescence lifetime of the excited molecule. Therefore, the decay profile was fitted with biexponential function with χ^2 value close to unity [50]. The fluorescence lifetime of the dye was calculated in a different solvent using eqn. 5:

$$I(t) = (A_1\tau_1 + A_2\tau_2) \quad (5)$$

where τ_1 and τ_2 represented the short and longer lifetime components with their normalized amplitude components A_1 and A_2 , respectively, and the average fluorescence lifetime of the CMI dye in different solvents are given in Table-1.

The fluorescence decay profile of CMI dye was recorded in DMSO and is shown in Fig. 3 along with weighted residual plot. The fluorescence decay profile of CMI dye in DMSO is best fitted with a bi-exponential fitting model with χ^2 value is equal to 1.16, similarly fluorescence decay profile of CMI dye is recorded in different solvents and their fluorescence lifetime along with χ^2 values are given in Table-1. It is observed that on changing media from non-polar to polar, fluorescence lifetime increases from 2.83 ns to 2.98 ns. These results clearly suggest that the solvent polarity increase excited state lifetime of the electron. This is probably a direct result of an increase in the vibrational deactivation because of the increase in the vibronic mode degrees of freedom, which also supported by decrease in magnitude of non-radiative rate constant upon increase in the solvent polarity [51].

The ground state optimized molecular structures of CMI dye is shown in Fig. 4. The highest occupied molecular orbital (HOMO) and lowest unoccupied molecular orbital (LUMO) of CMI dye in gaseous phase is shown in Fig. 5. The theoretically calculated values of HOMO, LUMO and energy band gap of CMI dye in different solvents are given in Table-2. It is observed that the energy band gap decreases with increase solvent polarity. The luminescence property of organic molecule can be predicated based on the spatial distribution of molecular mainly

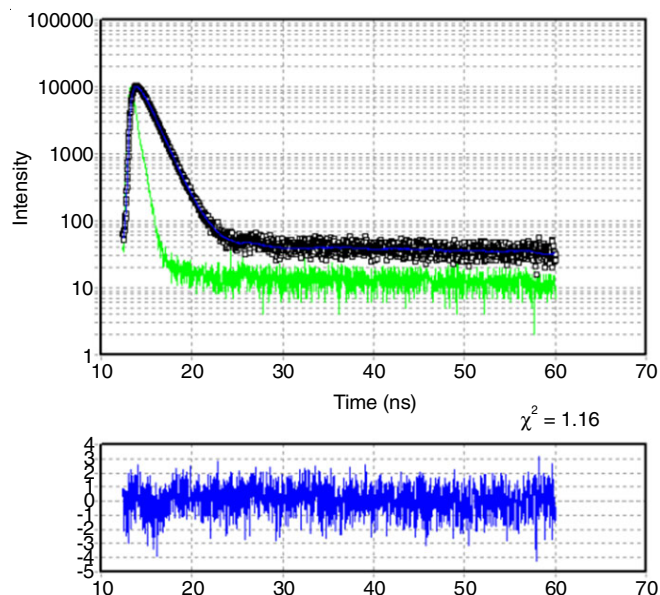


Fig. 3. Fluorescence decay profile of CMI dye (1×10^{-5} M) excited at 361 nm along with weighted residual plot in DMSO

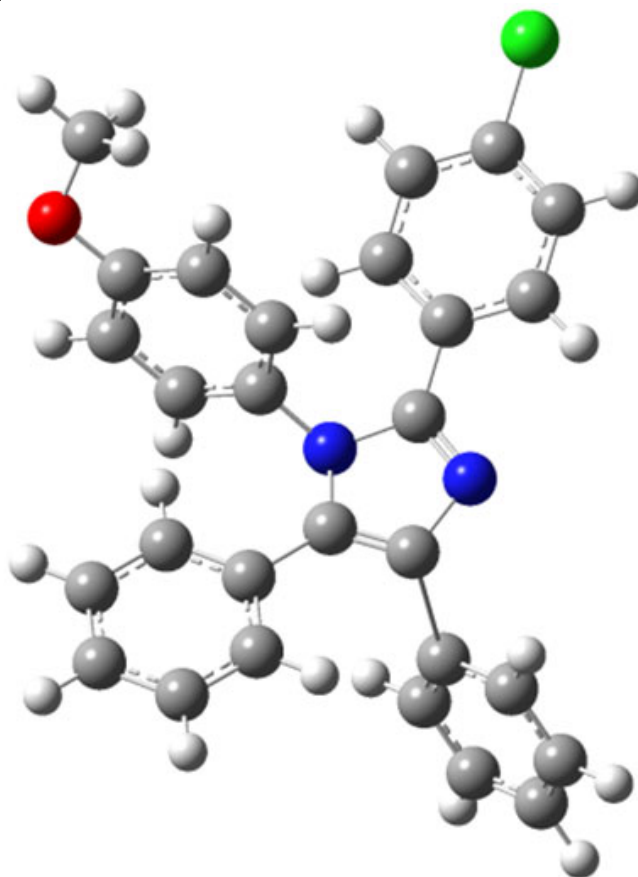


Fig. 4. Optimized molecular geometry of CMI dye molecule

orbitals, those of HOMO and LUMO. The synthesized molecule shows large HOMO value and small energy band gap which is essential properties for DSSC due to the strong electron accepting ability of the electron-acceptor group is fundamentally a consequence of the large stabilization of LUMO causes lowering of the HOMO-LUMO gap. Fig. 5 showed that the CMI dye

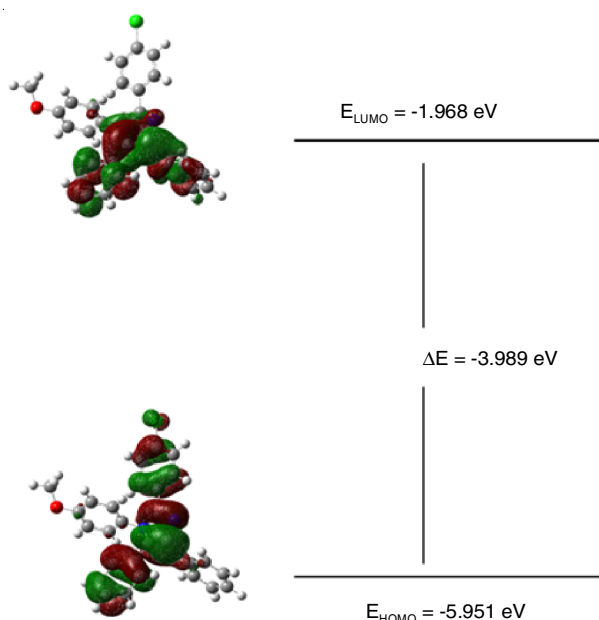


Fig. 5. Molecular orbital amplitude plots of HOMO and LUMO levels of CMI dye molecule in gaseous phase

in gaseous phase the electron clouds of HOMO energy levels are all mainly located on 2-(4-chlorophenyl)-4-phenyl-2H and this data strongly counts for good electron donating property of unit and LUMO energy levels are mainly concentrated on 4,5-diphenyl-2H-imidazole unit, which is useful in the application of DSSC due to an increase in the enhancement of electron transfer. The HOMO-LUMO values obtained by theoretical and experimental cyclic voltammetric analysis methods are in good agreement with each other.

Chemical hardness is one of the important parameters in order to explore organic molecule in the field of optoelectronic. The chemical hardness (η) of the molecule can be calculated by using these HOMO-LUMO energy values. To denote resistance to deformation by mechanical force the hardness and softness are suggested [48]. Molecules with large HOMO-LUMO gap is hard, which implies higher stability and opposing charge transfer since they oppose changes in their electron density and distribution. On contrary, molecules that require a small energy gap for its excitation are also termed as soft molecules. Hence, they are highly polarizable in nature [50].

The chemical hardness (η) can be calculated using eqn. 6:

$$\eta_{\text{hard}} = \frac{[E_L - E_H]}{2} \quad (6)$$

where, E_H and E_L is the energy value of HOMO and LUMO, respectively. The chemical hardness values calculated from the theoretical and experimental methods are shown in Table-2. Thus, it was observed that the small value of η and HOMO-LUMO energy gaps reflects that molecule are in soft in nature.

The molecular electrostatic potential map (MEPM) of the compound was used to find out the reactive sites for electrophilic and nucleophilic attacks and also useful in biological detection and hydrogen bonding interactions studies [52,53]. In addition, the MEPM is based on the molecular size, shape as well as positive, negative and neutral electrostatic potential region in terms of colour grading. The different values of the electrostatic potential at the surface are represented by different colours; red represents regions of most negative electrostatic potential, blue represents regions of most positive electrostatic potential [48]. It also provides an understanding of the relative polarity of the molecule.

In order to know the charge interrelated properties of the CMI dye, molecular electrostatic potential maps were plotted and are shown in Fig. 6. It was observed that the positive phases (blue colour) around the imidazole ring which consists of a nitrogen atom and all hydrogen atoms, whereas negative phases around the methoxy group.

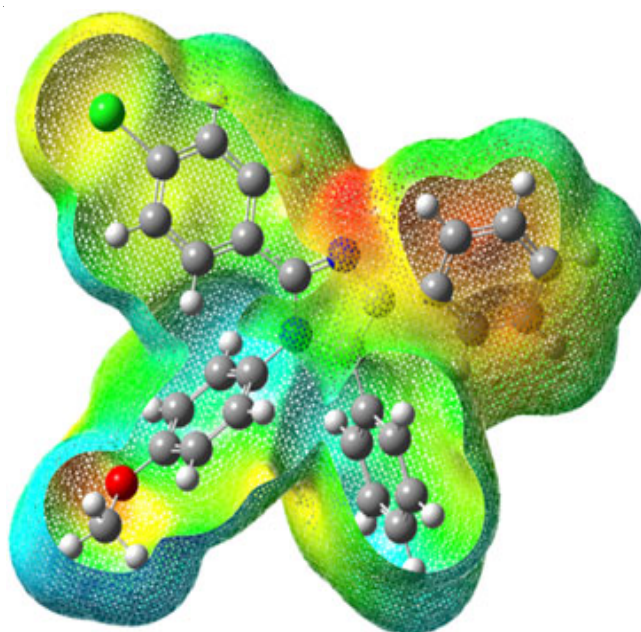


Fig. 6. Molecular electrostatic potential map of CMI dye

Thermogravimetric analysis (TGA): The CMI dye was subjected to thermogravimetric analysis in the temperatures ranged from room temperature to 350 °C under nitrogen atmosphere. The TGA results revealed that first degradation was observed in the range of 35-70 °C with minor weight loss (1.27%) due to the evaporation of moisture content in the compounds. The major weight loss was observed in the range of 144-184 °C (Fig. 7). The thermal and morphological stabilities values of CMI dye is summarized in Table-3. These results revealed that the CMI dye has good thermal stability, which can be used in the construction of the dye sensitized solar cells [54].

TABLE-3
THERMAL AND MORPHOLOGICAL STABILITIES OF CMI DYE

Dye	I-Degradation (% wt loss)	II-Degradation (% wt loss)	III-Degradation (% wt loss)
CMI	144.74to 184.11 °C (1.410 %)	238.52to255.55 °C (1.185%)	268.78to269.62 °C (0.850%)

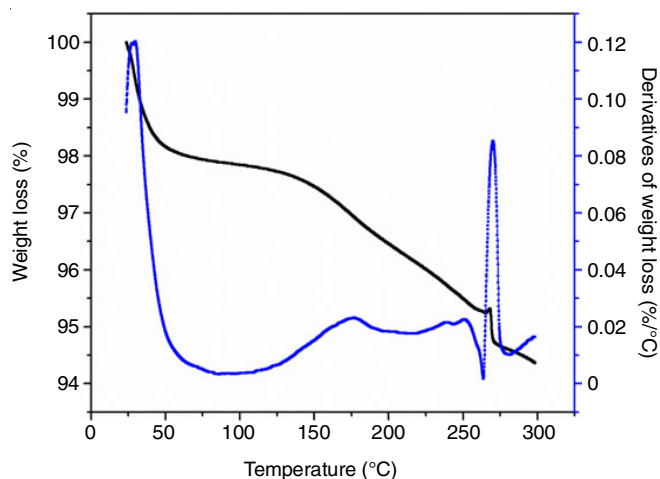


Fig. 7. TGA/Derivative TGA thermograms of the CMI dye measured at a heating rate of $10\text{ }^{\circ}\text{C min}^{-1}$ under nitrogen atmosphere

Spectroscopic studies: The absorption spectrum of CMI dye of concentration $1 \times 10^{-4}\text{ M}$ in the absence and presence of TiO_2 nanoparticles is recorded in acetonitrile at room temperature. From Fig. 8, it was observed that the absorption spectra of CMI dye increase with the increase in concentration of TiO_2 nanoparticles broadening of spectra without shifting the peak position and no new absorption peak is observed. This result revealed that the formation of a ground-state complex between CMI dye TiO_2 nanoparticles was prohibited [54].

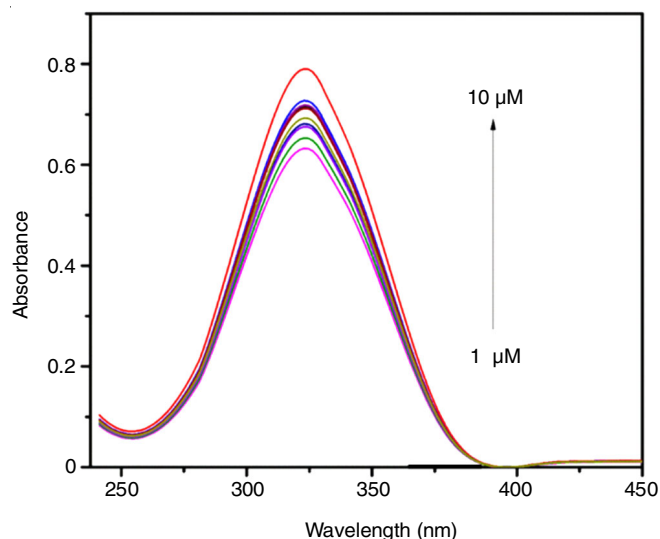


Fig. 8. Absorption spectra of CMI dye in acetonitrile in the absence and presence of TiO_2 nanoparticles

The steady state fluorescence and time resolved fluorescence spectra of CMI dye were recorded in the absence and presence of TiO_2 nanoparticles in acetonitrile at room temperature (Figs. 9 and 10). Table-4 represents the fluorescence intensity and lifetime values of CMI dye in the absence and presence of TiO_2 nanoparticles. From Table-4, it was observed that fluorescence lifetime and intensity decrease with increasing concentration of TiO_2 nanoparticles. These spectral behaviours can be analyzed using the Stern-Volmer relation [50] and are given in eqns. 7 and 8.

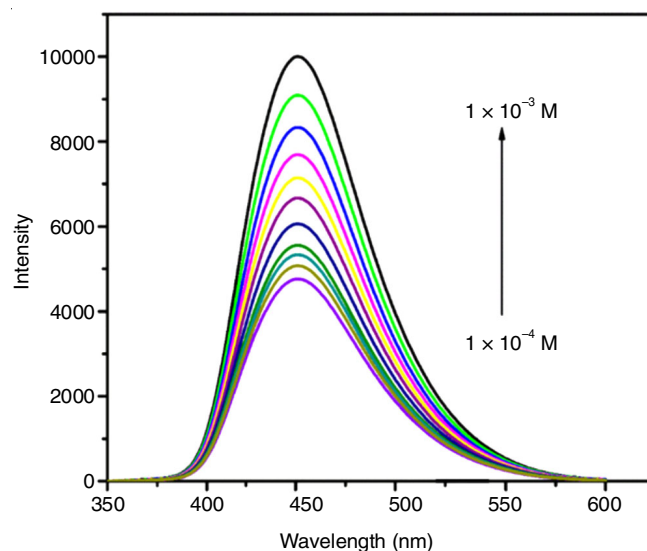


Fig. 9. Steady state fluorescence spectra of CMI dye in the absence and presence of TiO_2 nanoparticles in acetonitrile excited at 329 nm

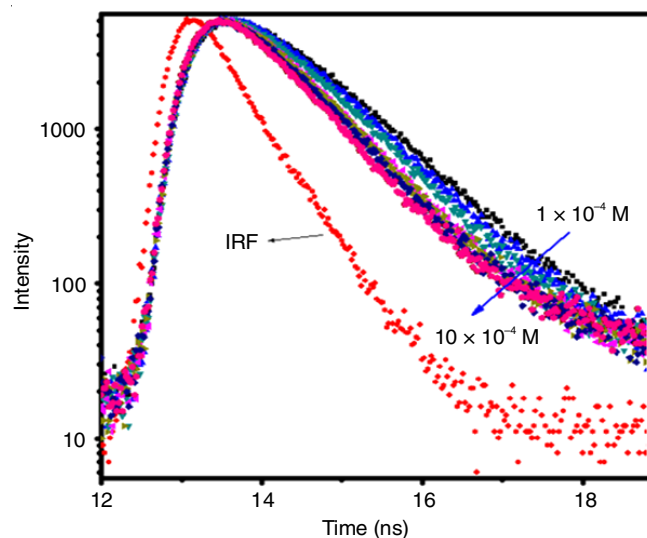


Fig. 10. Fluorescence decay curve of CMI dye in the absence and presence of TiO_2 nanoparticles in acetonitrile

TABLE-4
VALUES OF TiO_2 CONCENTRATIONS, FLUORESCENCE INTENSITY AND FLUORESCENCE LIFETIME OF CMI DYE WITH CORRESPONDING χ^2 VALUES

TiO_2 NPs concentration $\times 10^{-4}\text{ M}$	Fluorescence intensity of CMI	Fluorescence lifetime of CMI (ns)	χ^2
0	10000	2.98	1.11
1	9112	2.96	1.15
2	8355	2.92	1.11
3	7700	2.89	1.09
4	7165	2.85	1.12
5	6697	2.82	1.11
6	6083	2.80	1.15
7	5578	2.76	1.18
8	5361	2.75	1.13
9	5109	2.73	1.11
10	4789	2.71	1.11

$$\frac{I_0}{I} = 1 + k_{sv}[\text{TiO}_2] \quad (7)$$

$$\frac{\tau_0}{\tau} = 1 + k_{sv}[\text{TiO}_2] \quad (8)$$

where, I_0 or τ_0 are the fluorescence intensities or lifetime of CMI dye in the absence of TiO_2 nanoparticles. I or τ are the fluorescence intensities or lifetime of CMI dye in the presence of TiO_2 nanoparticles.

Using steady state and time resolved fluorescence value of CMI dye Stern-Volmer (S-V) plot was drawn and is shown in Fig. 11. The values of S-V constant and bimolecular quenching are tabulated in Table-5. The S-V plot found to linear with intercept equal to unity and also variation in S-V constant obtained from both methods suggest that the fluorescence quenching was due to combined dynamic and static quenching process.

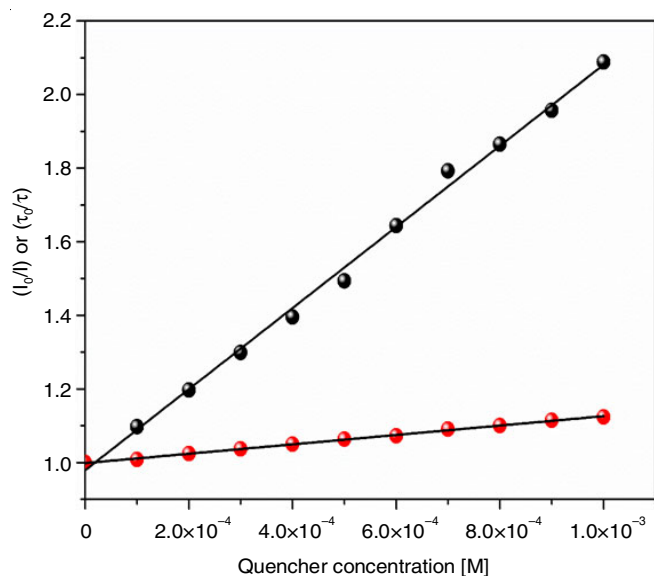


Fig. 11. Steady state and time resolved S-V Plot of CMI dye

The magnitudes of bimolecular quenching constant obtained from both the methods suggest that short range interactions were occurred between CMI dye and TiO_2 nanoparticles. Further, stoichiometry and the association constant (K_a) of CMI dye with TiO_2 nanoparticles were estimated from Benesi-Hilderbrand equation (eqn. 9) [55]:

$$\frac{1}{(I-I_0)} = \frac{1}{K_a[C][Q]} + \frac{1}{[C]} \quad (9)$$

Here all the terms in eq. 9 have their usual meaning. The $1/[Q]$ vs. $1/(I-I_0)$ plots for CMI dye- TiO_2 nanoparticles systems

are shown in Fig. 12. Benesi-Hilderbrand plot was perfectly linear and hence provided the evidence for the 1:1 stoichiometry between CMI dye and TiO_2 nanoparticles. The association constant (K_a) was calculated by the ratio of intercept to slope and the values are given in Table-5. The K_a value is almost in the same range (10^2) of the reported values [55,56].

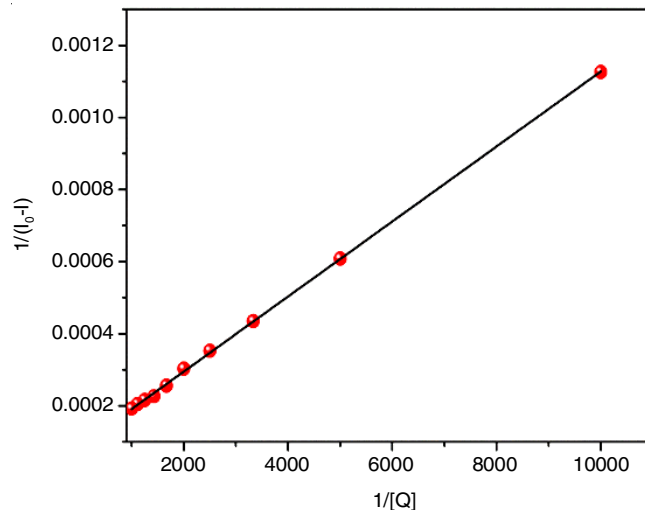


Fig. 12. Benesi-Hilderbrand linear analysis plot of all solute with varying concentration of TiO_2 nanoparticles in acetonitrile

The absorption and emission spectra of CMI dye (Fig. 14) suggest that the non-overlap between absorption spectra of TiO_2 nanoparticles and emission spectra of CMI dye. This also suggests the possibility of resonance energy transfer between CMI dye and TiO_2 nanoparticles is ruled out. Using Rehm-Weller relation the energy transfer from CMI dye to TiO_2 nanoparticles can be estimated. The Rehm-Weller equation (eqn. 10) [57] as follows:

$$\Delta G_{et} = E_{1/2}^{ox} + E_{1/2}^{red} + E_s + C \quad (10)$$

where, $E_{1/2}^{ox}$ is the oxidation potential of CMI dye; $E_{1/2}^{red}$ is the reduction potential of TiO_2 ; E_s is the excited singlet state energy of CMI dye and C is the coulombic term.

The cyclic voltammogram (CV) of CMI dye in acetonitrile and DMSO have been displayed in Figs. 13 and 14. From cyclic voltammogram, the oxidation potentials of CMI dye were found to be 1.164 V and 1.012 V for DMSO and acetonitrile, respectively. The E_s values of CMI dye were 3.272 eV and 3.255 eV for acetonitrile and DMSO, respectively. Reduction potential of TiO_2 was obtained from the literature which is -0.5 V [58,59]. Substituting the values of E_s in Eq.10, ΔG_{et} values for acetonitrile and DMSO were determined as -3.936 eV and -3.767 eV, respectively and coulombic term was neglected

TABLE-5
VALUES OF STERN-VOLMER CONSTANT, BIMOLECULAR QUENCHING CONSTANT AND ASSOCIATION CONSTANT OF CMI DYE

Solvent	Steady state method			Time resolved method	
	Stern-Volmer constant (k_{sv}) $\times 10^3 \text{ M}^{-1}$	Bimolecular quenching constant (k_q) $\times 10^{11} \text{ M}^{-1} \text{ s}^{-1}$	Association constant (K_a) $\times 10^2 \text{ M}^{-1}$	Stern-Volmer constant (k'_{sv}) $\times 10^2 \text{ M}^{-1}$	Bimolecular quenching constant (k'_q) $\times 10^{10} \text{ M}^{-1} \text{ s}^{-1}$
Dimethyl sulfoxide	1.101	3.932	7.900	1.27	4.261

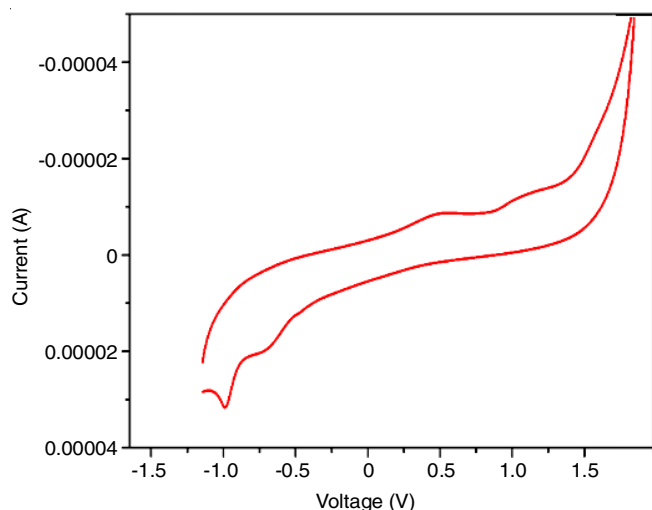


Fig. 13. Cyclic voltammetric curves of CMI dye were measured in acetonitrile in the presence of $n\text{-Bu}_4\text{NPF}_6$ at a scan rate of 100 mV s^{-1}

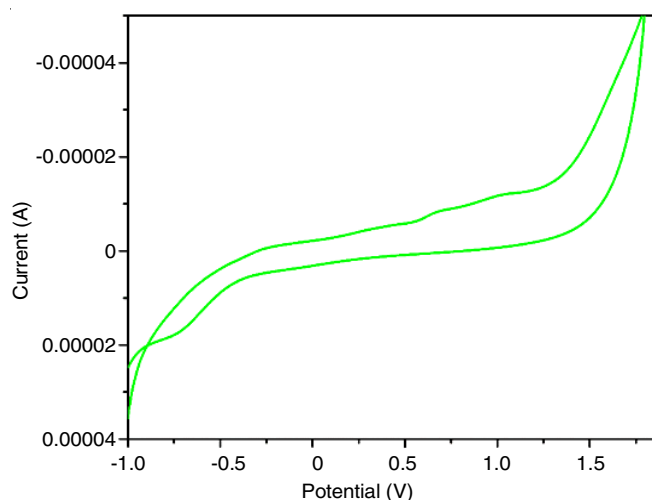


Fig. 14. Cyclic voltammetric curves of CMI dye were measured in DMSO in the presence of $n\text{-Bu}_4\text{NPF}_6$ at a scan rate of 100 mV s^{-1}

since in polar solvents coulombic term was very small. From the magnitudes of ΔG_{et} , it is observed that ΔG_{et} is greater in acetonitrile than DMSO indicating prominent thermodynamically favourable electron transfer process from CMI dye to TiO_2 nanoparticles in acetonitrile than DMSO. These observations are the preliminary indications for the transfer of photogenerated electrons from CMI dye to TiO_2 nanoparticles and thus prompt us to fabricate DSSC.

Fabrication of dye-sensitized solar cell: Commercial TiO_2 nanopowder (P25) was mixed in α -terpineol and ethyl cellulose to form TiO_2 paste. About $10 \mu\text{m}$ thick TiO_2 layer was coated on FTO with an active area of 0.25 cm^2 by doctor-blade technique. The TiO_2 photo-anode was annealed at 500°C for 30 min and then soaked for sensitization at room temperature for 12 h in 10 mM of dye dissolved in *tert*-butyl alcohol and acetonitrile solution (1:1). A counter electrode was prepared by doctor-blade coating of platinum paste on to the FTO surface, which was annealed at 400°C for 10 min. A $25 \mu\text{m}$ thick Surlyn film was used to fabricate cell. DSSC was completed upon the injection of the electrolyte through the pre-drilled hole.

Photo-electrochemical measurement: The electrochemical properties of CMI were explored by cyclic voltammetry (CV). The HOMO-LUMO band gap was derived from the difference between HOMO and LUMO energy levels. HOMO energy levels were calculated using the following equation

$$\text{HOMO} = -[E_{\text{OX}}^{\text{ONSET}} + 4.44] \quad (11)$$

The lowest unoccupied molecular orbital (LUMO) is equal to HOMO level minus Zero-zeroth energy (ΔE_{00}). Whereas, zero-zeroth energy ($\Delta E_{00} = 1240/\lambda$) of CMI dye alone is the intersection of the normalized absorption and fluorescence spectra (Fig. 15) and was found as 3.139 eV. Thus, LUMO level was found to be -2.312 V , which lies well above the conduction band edge of TiO_2 (-0.5 V vs. NHE), ensuring the required driving force for electron injection from the dye into the TiO_2 semiconductor. Fig. 16 shows the schematic theoretical energy level diagram of each component of dye sensitized TiO_2 electrode. Therefore, solar cell sensitized by CMI dye was thus fabricated in order to investigate the solar to electricity conversion efficiency.

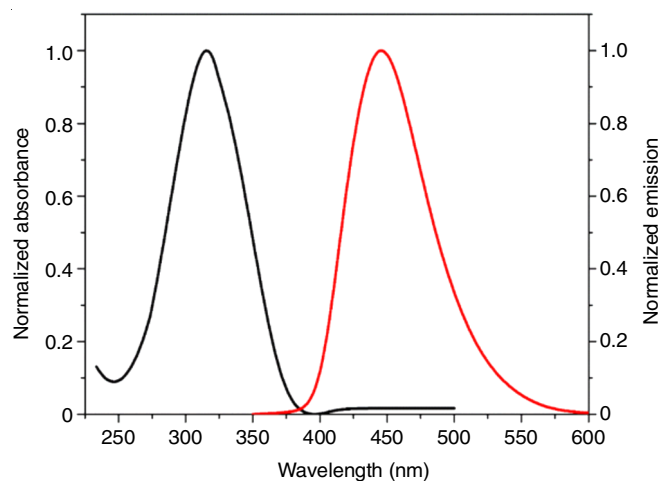


Fig. 15. Normalized absorption and emission spectra of CMI dye in acetonitrile

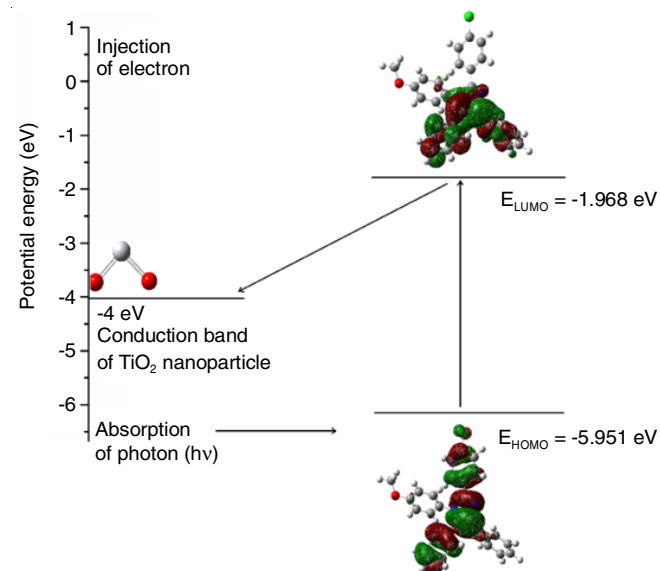


Fig. 16. Schematic energy level diagram of photo induced electron transfer from CMI dye to TiO_2 nanoparticles

The I-V characteristics of DSSCs were measured in the dark and under simulated solar light conditions. NREL certified silicon photodiode was used to calibrate output power to one sun. The conversion efficiency of DSSC based on the photocurrent vs. voltage (I-V) curve was recorded with a Keithley source meter.

The conversion efficiency (η) and fill factor (FF) were calculated according to eqns. 12 and 13, respectively

$$\eta = \frac{J_{sc} V_{oc} FF}{I_0} \times 100 \quad (12)$$

$$FF = \frac{V_{max} \times iV_{max}}{J_{sc} \times iV_{oc}} \quad (13)$$

where, V_{oc} , J_{sc} , V_{max} , J_{max} and I_0 are the open circuit voltage, short circuit current density, maximum power point voltage, maximum power point current density and total incident irradiance ($I_0 = 1000 \text{ W/m}^2$), respectively. The plots of photocurrent density (J) versus voltage (V) are shown in Fig. 17. and the values of V_{oc} , J_{sc} , η and FF are shown in Table-6. Photovoltaic conversion efficiency (η) of DSSCs sensitized with CMI dyes is 1.76% under AM 1.5 irradiation (1000 W/m^2). The photovoltaic conversion efficiency of CMI dye is lower than the standard dye may be due to the lower value of the molar extinction coefficient of CMI dye and may be due to some other regions, which need further investigations.

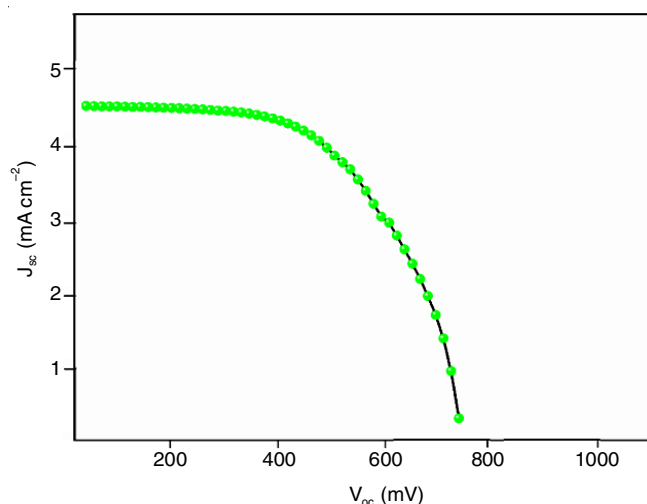


Fig. 17. Photo-current density-voltage (J-V) characteristics of the best performed DSSC's bath CMI dye

TABLE-6
OPTIMIZED PHOTOVOLTAIC
PARAMETERS VALUES OF CMI DYE

Dye	V_{oc} (mV)	J_{sc} (mA cm ⁻²)	FF	η
CMI	653	4.74	56.73	1.76

Conclusion

In the present work, a D- π -A substituted imidazole derivative (CMI) was successfully synthesized. The photophysical properties of CMI dye were calculated using the experimental and theoretical techniques. Further, the effect of TiO₂ nano-

particles on CMI dye has been studied using spectroscopic and electrochemical investigations. For completeness, the association constant has been calculated from Benesi-Hilderbrand relation and it suggests that there is a possibility of interaction between CMI dye and TiO₂ nanoparticles. Fluorescence quenching of CMI dye in the presence TiO₂ nanoparticles is due to combine static and dynamic quenching. The Rehm-Weller theory infers that thermodynamically favourable electron transfer takes place between CMI dye to TiO₂ nanoparticles. Thus, the solar energy harvesting process has been investigated by using TiO₂-CMI dye fabricated solar cell. The photovoltaic conversion efficiency and fill factor of fabricated DSSC were found to be 1.76% and 0.56, respectively. Further improvement of power conversion efficiency of DSSC may be achieved with further optimization of solar cell parameters.

ACKNOWLEDGEMENTS

One of the authors, (K.M. Mahadevan) is thankful to The Department of Science and Technology, Ministry of Science and Technology, India for financial supports. The authors are also thankful to the authorities of USIC, Karnatak University, Dharwad, India for providing the instrumental facilities for this research work.

CONFLICT OF INTEREST

The authors declare that there is no conflict of interests regarding the publication of this article.

REFERENCES

1. A. Mishra, M.K.R. Fischer and P. Bauerle, *Angew. Chem. Int. Ed.*, **48**, 2474 (2009); <https://doi.org/10.1002/anie.200804709>
2. A. Mishra and P. Bauerle, *Angew. Chem. Int. Ed.*, **51**, 2020 (2012); <https://doi.org/10.1002/anie.201102326>
3. H. Li, Y. Hou, Y. Yang, R. Tang, J. Chen, H. Wang, H. Han, T. Peng, Q. Li and Z. Li, *ACS Appl. Mater. Interfaces*, **5**, 12469 (2013); <https://doi.org/10.1021/am403668d>
4. Z. Wang, M. Liang, L. Wang, Y. Hao, C. Wang, Z. Sun and S. Xue, *Chem. Commun.*, **49**, 5748 (2013); <https://doi.org/10.1039/c3cc42121j>
5. K.S.V. Gupta, T. Suresh, S.P. Singh, A. Islam M. Chandrasekharam and L. Han, *Org. Electron.*, **15**, 266 (2014); <https://doi.org/10.1016/j.orgel.2013.11.020>
6. A. Venkateswararao, K.R.J. Thomas, C.P. Lee, C.T. Li and K.C. Ho, *ACS Appl. Mater. Interfaces*, **6**, 2528 (2014); <https://doi.org/10.1021/am404948w>
7. D. Cao, J. Peng, Y. Hong, X. Fang, L. Wang and H. Meier, *Org. Lett.*, **13**, 1610 (2011); <https://doi.org/10.1021/ol2000167>
8. M. Marszalek, S. Nagane, A. Ichake, R. Humphry-Baker, V. Paul, S.M. Zakeeruddin and M. Gratzel, *RSC Adv.*, **3**, 7921 (2013); <https://doi.org/10.1039/c3ra22249g>
9. Z.S. Wang, Y. Cui, K. Hara, Y. Dan-oh, C. Kasada and A. Shinpo, *Adv. Mater.*, **19**, 1138 (2007); <https://doi.org/10.1002/adma.200601020>
10. B. Liu, B. Wang, R. Wang, L. Gao, S. Huo, Q. Liu, X. Li and W. Zhu, *J. Mater. Chem. A Mater. Energy Sustain.*, **2**, 804 (2014); <https://doi.org/10.1039/C3TA13993J>
11. Q. Chai, W. Li, S. Zhu, Q. Zhang and W. Zhu, *ACS Sustain. Chem. Eng.*, **2**, 239 (2014); <https://doi.org/10.1021/sc400293v>
12. X.H. Zhang, Y. Cui, R. Katoh, N. Koumura and K. Hara, *J. Phys. Chem. C*, **114**, 18283 (2010); <https://doi.org/10.1021/jp105548u>

13. L. Yu, J. Xi, H.T. Chan, T. Su, L.J. Antrobus, B. Tong, Y. Dong, W.K. Chan and D.L. Phillips, *J. Phys. Chem. C*, **117**, 2041 (2013); <https://doi.org/10.1021/jp3113182>
14. A. Yella, R. Humphry-Baker, B.F.E. Curchod, N. Ashari Astani, J. Teuscher, L.E. Polander, S. Mathew, J.-E. Moser, I. Tavernelli, U. Rothlisberger, M. Grätzel, M.K. Nazeeruddin and J. Frey, *Chem. Mater.*, **25**, 2733 (2013); <https://doi.org/10.1021/cm401593b>
15. Y.-C. Chen, Y.-H. Chen, H.-H. Chou, S. Chaurasia, Y.S. Wen, J.T. Lin and C.-F. Yao, *Chem. Asian J.*, **7**, 1074 (2012); <https://doi.org/10.1002/asia.201100972>
16. R.Y.Y. Lin, Y.S. Yen, Y.T. Cheng, C.P. Lee, Y.C. Hsu, H.H. Chou, C.Y. Hsu, Y.C. Chen, J.T. Lin, K.C. Ho and C. Tsai, *Org. Lett.*, **14**, 3612 (2012); <https://doi.org/10.1021/ol301374c>
17. G. Marzari, J. Durantini, D. Minudri, M. Gervaldo, L. Otero, F. Fungo, G. Pozzi, M. Cavazzini, S. Orlandi and S. Quici, *J. Phys. Chem. C*, **116**, 21190 (2012); <https://doi.org/10.1021/jp305884u>
18. Z. Ci, X. Yu, C. Wang, T. Ma and M. Bao, *Dyes Pigments*, **104**, 8 (2014); <https://doi.org/10.1016/j.dyepig.2013.12.020>
19. D. Heredia, J. Natera, M. Gervaldo, L. Otero, F. Fungo, C.Y. Lin and K.T. Wong, *Org. Lett.*, **12**, 12 (2010); <https://doi.org/10.1021/ol902314z>
20. L. Macor, M. Gervaldo, F. Fungo, L. Otero, T. Dittrich, C.Y. Lin, F.C. Chi, S.W. Fang, K.T. Lii, K.-T. Wong, C.-H. Tsai and C.-C. Wu, *RSC Adv.*, **2**, 4869 (2012); <https://doi.org/10.1039/c2ra00995a>
21. R. Yeh-Yung Lin, H.-W. Lin, Y.-S. Yen, C.-H. Chang, H.-H. Chou, P.-W. Chen, C.-Y. Hsu, Y.-C. Chen, J.T. Lin and K.-C. Ho, *Energy Environ. Sci.*, **6**, 2477 (2013); <https://doi.org/10.1039/c3ee41075g>
22. Y.Z. Lin, C.H. Huang, Y.J. Chang, C.W. Yeh, T.M. Chin, K.M. Chi, P.T. Chou, M. Watanabe and T.J. Chow, *Tetrahedron*, **70**, 262 (2014); <https://doi.org/10.1016/j.tet.2013.11.072>
23. J. Liu, R. Li, X. Si, D. Zhou, Y. Shi, Y. Wang, X. Jing and P. Wang, *Energy Environ. Sci.*, **3**, 1924 (2010); <https://doi.org/10.1039/c0ee00304b>
24. M.K.R. Fischer, S. Wenger, M. Wang, A. Mishra, S.M. Zakeeruddin, M. Grätzel and P. Bauerle, *Chem. Mater.*, **22**, 1836 (2010); <https://doi.org/10.1021/cm903542v>
25. Q. Feng, Q. Zhang, X. Lu, H. Wang, G. Zhou and Z.S. Wang, *ACS Appl. Mater. Interfaces*, **5**, 8982 (2013); <https://doi.org/10.1021/am402036j>
26. H. Choi, I. Raabe, D. Kim, F. Teocoli, C. Kim, K. Song, J.H. Yum, J. Ko, M.K. Nazeeruddin and M. Grätzel, *Chem. Eur. J.*, **16**, 1193 (2010); <https://doi.org/10.1002/chem.200902197>
27. C.Y. Chen, N. Postrakulchote, T.H. Hung, C.J. Tan, H.H. Tsai, S.M. Zakeeruddin, C.G. Wu and M. Grätzel, *J. Phys. Chem. C*, **115**, 20043 (2011); <https://doi.org/10.1021/jp206312g>
28. T.H. Kwon, V. Armel, A. Nattestad, D.R. MacFarlane, U. Bach, S.J. Lind, K.C. Gordon, W. Tang, D.J. Jones and A.B. Holmes, *J. Org. Chem.*, **76**, 4088 (2011); <https://doi.org/10.1021/jo2001484>
29. A. Venkateswararao, K.R.J. Thomas, C.P. Lee and K.C. Ho, *Tetrahedron Lett.*, **54**, 3985 (2013); <https://doi.org/10.1016/j.tetlet.2013.05.069>
30. T. Sudyoadsuk, S. Pansay, S. Morada, R. Rattanawan, S. Namuangruk, T. Kaewin, S. Jungstittiwong and V. Promarak, *Eur. J. Org. Chem.*, **2013**, 5051 (2013); <https://doi.org/10.1002/ejoc.201300373>
31. Y. Hong, J.Y. Liao, D. Cao, X. Zhang, D.B. Kuang, L. Wang, H. Meier and C.Y. Su, *J. Org. Chem.*, **76**, 8015 (2011); <https://doi.org/10.1021/jo201057b>
32. W. Lee, S.B. Yuk, J. Choi, H.J. Kim, H.W. Kim, S.H. Kim, B. Kim, M.J. Ko and J.P. Kim, *Dyes Pigments*, **102**, 13 (2014); <https://doi.org/10.1016/j.dyepig.2013.10.005>
33. Y. Hua, S. Chang, D. Huang, X. Zhou, X. Zhu, J. Zhao, T. Chen, W.Y. Wong and W.K. Wong, *Chem. Mater.*, **25**, 2146 (2013); <https://doi.org/10.1021/cm400800h>
34. C. Chen, X. Yang, M. Cheng, F. Zhang, J. Zhao and L. Sun, *ACS Appl. Mater. Interfaces*, **5**, 10960 (2013); <https://doi.org/10.1021/am403210v>
35. M. Velusamy, K.R. Justin Thomas, J.T. Lin, Y.-C. Hsu and K.-C. Ho, *Org. Lett.*, **7**, 1899 (2005); <https://doi.org/10.1021/ol050417f>
36. S. Haid, M. Marszalek, A. Mishra, M. Wielopolski, J. Teuscher, J.-E. Moser, R. Humphry-Baker, S.M. Zakeeruddin, M. Grätzel and P. Bäuerle, *Adv. Funct. Mater.*, **22**, 1291 (2012); <https://doi.org/10.1002/adfm.201102519>
37. M. Zhang, Y. Wang, M. Xu, W. Ma, R. Li and P. Wang, *Energy Environ. Sci.*, **6**, 2944 (2013); <https://doi.org/10.1039/c3ee42331j>
38. Y. Cui, Y. Wu, X. Lu, X. Zhang, G. Zhou, F.B. Miaephe, W. Zhu and Z.-S. Wang, *Chem. Mater.*, **23**, 4394 (2011); <https://doi.org/10.1021/cm202226j>
39. Y.S. Yen, C.T. Lee, C.Y. Hsu, H.H. Chou, Y.C. Chen and J.T. Lin, *Chem. Asian J.*, **8**, 809 (2013); <https://doi.org/10.1002/asia.201201173>
40. M. Velusamy, Y.C. Hsu, J.T. Lin, C.W. Chang and C.P. Hsu, *Chem. Asian J.*, **5**, 87 (2010); <https://doi.org/10.1002/asia.200900244>
41. L. Zhou, C. Jia, Z. Wan, Z. Li, J. Bai, L. Zhang, J. Zhang and X. Yao, *Dyes Pigments*, **95**, 743 (2012); <https://doi.org/10.1016/j.dyepig.2012.05.007>
42. L. Zhou, C. Jia, Z. Wan, X. Chen and X. Yao, *Org. Electron.*, **14**, 1755 (2013); <https://doi.org/10.1016/j.orgel.2013.04.004>
43. M. Mao, J.B. Wang, Z.F. Xiao, S.Y. Dai and Q.H. Song, *Dyes Pigments*, **94**, 224 (2012); <https://doi.org/10.1016/j.dyepig.2012.01.011>
44. W. Lee, Y. Yang, N. Cho, J. Ko and J.I. Hong, *Tetrahedron*, **68**, 5590 (2012); <https://doi.org/10.1016/j.tet.2012.04.074>
45. D. Kumar, K.R.J. Thomas, C.P. Lee and K.C. Ho, *Org. Lett.*, **13**, 2622 (2011); <https://doi.org/10.1021/ol2006874>
46. J. Chang, C.P. Lee, D. Kumar, P.W. Chen, L.Y. Lin, K.R.J. Thomas and K.C.J. Ho, *Power Sources*, **240**, 779 (2013); <https://doi.org/10.1016/j.jpowsour.2013.04.075>
47. M.J. Frisch, G.W. Trucks, H.B. Schlegel, G.E. Scuseria, M.A. Robb, J.R. Cheeseman, G. Scalmani, V. Barone, B. Mennucci, G.A. Petersson, H. Nakatsuji, M. Caricato, X. Li, H.P. Hratchian, A.F. Izmaylov, J. Bloino, G. Zheng, J.L. Sonnenberg, M. Hada, M. Ehara, K. Toyota, R. Fukuda, J. Hasegawa, M. Ishida, T. Nakajima, Y. Honda, O. Kitao, H. Nakai, T. Vreven, J.A. Montgomery Jr., J.E. Peralta, F. Ogliaro, M. Bearpark, J.J. Heyd, E. Brothers, K.N. Kudin, V.N. Staroverov, T. Keith, R. Kobayashi, J. Normand, K. Raghavachari, A. Rendell, J.C. Burant, S.S. Iyengar, J. Tomasi, M. Cossi, N. Rega, J.M. Millam, M. Klene, J.E. Knox, J.B. Cross, V. Bakken, C. Adamo, J. Jaramillo, R. Gomperts, R.E. Stratmann, O. Yazyev, A.J. Austin, R. Cammi, C. Pomelli, J.W. Ochterski, R.L. Martin, K. Morokuma, V.G. Zakrzewski, G.A. Voth, P. Salvador, J.J. Dannenberg, S. Dapprich, A.D. Daniels, O. Farkas, J.B. Foresman, J.V. Ortiz, J. Cioslowski and D.J. Fox, Gaussian-09, Revision B.01, Gaussian, Inc., Wallingford, CT (2010).
48. L. Naik, C.V. Maridevarmath, I.A.M. Khazi and G.H. Malimath, *J. Photochem. Photobiol. Chem.*, **368**, 200 (2019); <https://doi.org/10.1016/j.jphotochem.2018.09.038>
49. L. Naik, N. Deshapande, I.A.M. Khazi and G.H. Malimath, *Braz. J. Phys.*, **48**, 16 (2018); <https://doi.org/10.1007/s13538-017-0540-x>
50. R.L. Joseph, Principles of Fluorescence Spectroscopy, Springer: New York, edn 3 (2006).
51. L.J. Cline Love, L.M. Upton and A.W. Ritter, Analytical Chemistry, vol. 50, Chap. 14, p. 2059 (1978).
52. J.S. Murray and K. Sen, Molecular Electrostatic Potentials: Concepts and Applications, Elsevier: Amsterdam (1996).
53. E. Scrocco and J. Tomasi, *Adv. Quantum Chem.*, **11**, 115 (1978); [https://doi.org/10.1016/S0065-3276\(08\)60236-1](https://doi.org/10.1016/S0065-3276(08)60236-1)
54. N. Deshapande, N.S. Belavagi, M.G. Sunagar, S. Gaonkar, G.H. Pujar, M.N. Wari, S.R. Inamdar and I.A.M. Khazi, *RSC Adv.*, **5**, 86685 (2015); <https://doi.org/10.1039/C5RA14550K>
55. L. Naik, I.A.M. Khazi and G.H. Malimath, *Optik*, **183**, 732 (2019); <https://doi.org/10.1016/j.ijleo.2019.02.145>
56. M.L. Benesi and J.H. Hildebrand, *J. Am. Chem. Soc.*, **71**, 2703 (1949); <https://doi.org/10.1021/ja01176a030>
57. D. Rehm and A. Weller, *Israel J. Chem.*, **8**, 259 (1970); <https://doi.org/10.1002/ijch.197000029>
58. X.X. Dai, H.L. Feng, Z.S. Huang, M.J. Wang, L. Wang, D.B. Kuang, H. Meier and D. Cao, *Dyes Pigments*, **114**, 47 (2015); <https://doi.org/10.1016/j.dyepig.2014.10.016>
59. P. Wang, S. Zakeeruddin, J. Moser and M. Grätzel, *J. Phys. Chem. B*, **107**, 13280 (2003); <https://doi.org/10.1021/jp0355399>